

What drives amyloid molecules to assemble into oligomers and fibrils?

Jeremy D. Schmit,* Kingshuk Ghosh, and Ken Dill†

*Department of Pharmaceutical Chemistry,
University of California, San Francisco, California 94158*

Abstract

We develop a general theory for three states of equilibrium of amyloid peptides: the monomer, oligomer, and fibril. We assume that the oligomeric state is a disordered micelle-like collection of a few peptide chains held together loosely by hydrophobic interactions into a spherical hydrophobic core. We assume that fibrillar amyloid chains are aligned and further stabilized by ‘steric zipper’ interactions – hydrogen bonding and steric packing, in addition to specific hydrophobic sidechain contacts. The model makes a broad set of predictions, consistent with experiments: (i) Similar to surfactant micellization, amyloid oligomerization should increase with bulk peptide concentration. (ii) The onset of fibrillization limits the concentration of oligomers in the solution. (iii) The average fibril length *vs.* monomer concentration agrees with data on α -synuclein, (iv) Full fibril length distributions follow those of α -synuclein, (v) Denaturants should ‘melt out’ fibrils, and (vi) Added salt should stabilize fibrils by reducing repulsions between amyloid peptide chains. Interestingly, small changes in solvent conditions can: (a) tip the equilibrium balance between oligomer and fibril, and (b) cause large changes in rates, through effects on the transition-state barrier. This model may provide useful insights into the physical processes underlying amyloid diseases.

PACS numbers:

*schmit@maxwell.ucsf.edu

†dill@maxwell.ucsf.edu

I. INTRODUCTION

What are the forces that stabilize aggregates of amyloid peptide molecules? This question is of interest because of the putative role played by amyloid aggregation in diseases such as Alzheimer’s, Parkinson’s, Mad Cow and type II diabetes [1]. Amyloid appears to aggregate into at least two different states: *amyloid oligomers*, which are small few-chain soluble disordered clusters, and *fibrils*, which are long many-chain highly structured β -sheet-like aggregates. The view has recently emerged that the oligomers may be the toxic species, not the fibrils, as had been expected because of the appearance of plaques in disease [2]. It has been challenging to understand the physical principles of amyloid aggregation, in part because of a lack of reductionist experimental model systems. In this breach, we believe that simple models can help guide and interpret experiments.

The first challenge is to disentangle how much of amyloid formation can be explained by equilibrium *vs.* kinetics. Often kinetics is easier to study experimentally because measuring rates does not require finding conditions of reversibility. Yet, there is experimental evidence of multiple stable states: monomers, oligomers, and fibrils, and perhaps a precursor to the fibrillar state, called the protofilament [3]. We believe insights can be gained from first understanding the underlying phase equilibria.

II. MODELING THE STATES OF AMYLOID AGGREGATION

We develop here a model of the equilibrium among the following states: (a) isolated monomeric amyloid peptide molecules in solution, (b) few-chain noncovalent aggregates (*oligomers*) of amyloid peptide molecules, (c) the single ‘macroscopic thread’ called a *protofilament*, which is a noncovalent ordered assembly of many chains, and (d) the *fibril*, which is a bundle of protofilaments. These states are shown schematically in Figs. 1 and 2. (In this paper, ‘monomer’ refers to an individual peptide chain, not to a single amino acid in a chain; see Fig. 2a) [3–5]. Our interest here is in peptides, such as $A\beta$, α -synuclein, and IAPP, that do not have single-chain native folded structures, so our model below neglects any possible additional equilibria with a native folded structure.

A. Modeling the oligomer state

The oligomer state is shown in Fig. 2a. For $A\beta$ aggregates, oligomers range in size from trimers to hundreds of monomers [3–5]. We model the amyloid oligomer state as a disordered spherical globule having a hydrophobic core containing N peptide chains. Each chain has L amino acids. We approximate the free energy of oligomerization, ΔF_{oligo} , from state A to B in Figure 2, in terms of the transfer of the NL amino acids from water into the oligomeric core as [6, 7],

$$\Delta F_{\text{oligo}} = \frac{\Delta F_{\text{AB}}}{kT} = -\chi NL, \quad (1)$$

where $kT\chi$ is the free energy of transfer per amino acid and χ is the Flory-Huggins parameter, averaged over the amino acid composition of the peptide and over the solvent accessibilities of the various amino acids. Following recent work [8], we neglect the distinction between interior and surface residues that was drawn in older models [6].

B. Modeling the protofilament and its nucleus

The β -sandwich motif, shown in Fig. 1c, is a common feature of amyloid aggregates observed in NMR and X-ray structures [9–12]. Here, we assume that the basic structural element comprising protofilaments and fibrils is the β -sandwich. Before describing our fibril model, we first define our terminology for structures throughout this paper. A β -strand is a single linear stretch of peptide chain. A β -sheet is comprised of two or more hydrogen-bonded β -strands (see Fig. 1a,b). A β -sandwich is two planar β -sheets face-to-face (see Fig. 1c). For example, in the fibrillar state the $A\beta$ molecule is a V -shaped β -hairpin comprised of two beta strands. In amyloid fibrils, the β -sandwich is stabilized by H-bonds parallel to the fibril axis and by hydrophobic and van der Waals interactions from the interdigitation of side chains within the steric zipper between the two β -strands (see Fig. 1c) [9]. At a given stage of fibrillization, we assume a β -sheet is composed of h β -strands. Each β strand contributes b amino acids to the β -sheet. The sheet width b must satisfy $b \leq \ell$, where $\ell \leq L$ is the length of the β -strands in the mature fibril. At a given stage of fibril formation, the total number of residues in the β state is $m = 2bh$, where the factor of two accounts for the two sheets in the β -sandwich. The quantities b and h are shown schematically in Fig. 2c,d. The quantity m serves as an order parameter for the extent of fibril formation.

We treat the equilibrium between the oligomer (state B in Fig. 2), the fibril nuclei (states C and D in Fig. 2), the protofilament (E in Fig. 2), and the full fibril (F in Fig. 2) in a way that resembles the standard treatment of the helix-coil transition in peptides [13–17].

We call the states $BCDE$ the *fibril ordering* pathway. The free energy is

$$\frac{\Delta F_{BCDE}(m)}{kT} = -\chi(NL - m) - m \ln g_s - \sqrt{\frac{m}{2}} \ln \gamma, \quad (2)$$

as a function of m , which can be regarded as an ‘order parameter’ or a ‘reaction coordinate’ along the route $BCDE$. m ranges from $m = 0$ when the system is fully disordered (*i.e.*, fully in state B), to $m = NL$ when the system is fully ordered in the β -state (*i.e.*, fully in state E). (So, in normalized form, a reaction coordinate could be expressed as $\xi = m/NL$). The first term in Eq. 2 is the free energy of converting m of the NL amino acids from their oligomeric disordered state, with a corresponding loss of the disordered micelle-like hydrophobic interactions.

The second term in Eq. 2, $-mkT \ln g_s$, is the free energy of forming m pairwise steric zipper interactions in the core of the fibril. g_s is a dimensionless propagation equilibrium coefficient. g_s resembles the quantity s in helix-coil theories [13, 16], except that g_s here describes β structure, not α -helical structure. g_s captures various types of interactions, including conformational entropy, hydrogen bonds, steric packing, and ordered sidechain hydrophobic interactions. A necessary condition for fibril formation is $g_s > 1$. That is, fibrils can only form when the sterically zipped state (hydrogen bonds, packing, and ordered hydrophobic interactions) is more favorable than the monomeric state. The subscript s here in g_s indicates an interaction within a single β -sandwich, not between the different β -sandwiches that make up a full fibril.

We treat fibrillar ordering as a surface/interior nucleation process. The third term in Eq. 2, $\sqrt{m/2} \ln \gamma$, is the free energy of initiating steric zipping at the edge of the β -sandwich (a square having $m/2$ residues, has a perimeter with $\sqrt{m/2}$ residues). In our model, γ , is a surface tension for forming the perimeter bonding. In the metaphor of helix-coil theories, γ resembles σ , the helix-coil nucleation parameter. Fig. 2 shows that the edge of the β -sandwich has $2b$ unsatisfied H-bonds, but only b unsatisfied hydrophobic contacts due to the stagger between the two sheets. It is these missing hydrophobic and H-bond interactions that account for why there should be a barrier, $\gamma < 1$, to nucleating the fibril. This nucleation barrier free energy in Eq. 2 is maximal for $b = \ell$. At the present stage of knowledge

of microscopic structures, this square-shape approximation has the advantage of simplicity and is adequate to capture the shift in the oligomer-fibril transition from hydrophobic to combined hydrophobic and hydrogen bonding interactions [18].

This model gives insight into fibril formation rates. We compute the free energy of the transition state by finding the maximum value of ΔF_{order} along the reaction coordinate m using Equation 2. The transition state is at $\Delta F^\ddagger = (d\Delta F_{\text{order}}/dm)_{m^*} = 0$, so given by

$$\frac{\Delta\Delta F^\ddagger}{kT} = \frac{\Delta F_{\text{order}}(m^*) - \Delta F_{\text{order}}(0)}{kT} = \frac{\ln^2 \gamma}{8(\ln(g_s) - \chi)}. \quad (3)$$

Eq. 3 shows that the free energy barrier will be extremely sensitive since the quantity $\ln(g_s) - \chi$ in the denominator will be small. $\ln g_s$ and χ are dimensionless quantities of order unity; their difference is small because the zipping free energy is expected to be only slightly more favorable than amorphous hydrophobic interactions. Small variations in g_s or χ , at the level of single amino-acid changes or slight changes in solution conditions, could change fibrillization rates by several orders of magnitude [19]. This provides a rationale for understanding how a single mutation could transform a normal fibrillization rate, which might be too slow to cause disease on a human lifetime, into a much faster fibrillization rate, sufficient to cause disease during a human lifetime.

Our model of the amyloid nucleation process differs from classic nucleation mechanisms in two respects: (1) ours involves a one-dimensional line tension, rather than a two-dimensional surface tension [20], and (2) our ordering transition is from oligomers to fibrils, not from monomers to aggregates, so our fibrillization mechanism is not driven by increasing the solution concentration of monomers. This is consistent with experiments showing that amyloid nucleation is concentration-independent. The proposed explanation in the Nucleated Conformational Conversion (NCC) model [21] is that oligomeric chains must enter an *activated conformation* to proceed to fibrils. In our model, the role of activation is played by the entropically unfavorable steric-zipper nucleus.

C. Modeling the full fibril

In our model, a full fibril consists of p β -sandwich-motif protofilaments stacked and bundled together. Fig. 2e shows such a fibril for $p = 2$. ΔF_{EF} is the free energy of bundling

protofilaments into fibrils,

$$\frac{\Delta F_{\text{bundling}}}{kT} = \frac{\Delta F_{\text{EF}}}{kT} = nL\epsilon = -nL \ln \left(\frac{g}{g_s} \right) \quad (4)$$

where L remains the number of amino acids per peptide chain. n is the number of peptide chains in the bundled fibril. g is the propagation constant for forming β structure in the mature fibril. Eq. 4 gives $-\ln g = -\ln g_s + \epsilon$, so $-\ln g_s$ is the free energy of the interactions within a single protofilament, and ϵ is the interaction energy holding the protofilaments together. Because these bundling interactions occur only between a subset of residues on the perimeter of the protofilament, we expect that g and g_s will be similar.

Peptides are frequently folded within a fibril such that a single peptide chain contributes multiple β -strands to the fibril. To account for this we introduce the parameters ℓ , the length of each β -strand, and n_s , the number of β strands formed by each peptide chain. For example, peptides such as $A\beta$ and IAPP that form a single hairpin in the mature fibril have $n_s = 2$. The quantity n_s , defined such that $L = n_s \ell$ is shown in Fig. 3.

From Eq. 2 it is clear that each protofilament will incur a nucleation penalty $-kT\ell \ln \gamma$ and each β -strand in the fibril will contribute a binding energy $-kT\ell \ln g$. However, a more convenient quantity is the binding energy per peptide $-kT\ell n_s \ln g = -kTL \ln g$. The free energy of a fibril consisting of n peptides is then

$$\frac{\Delta F_n}{kT} = \frac{\Delta F_{\text{AF}}}{kT} = -\ln(\gamma^{p\ell} g^{nL}). \quad (5)$$

The fibrillization index n must be greater than the minimum fibril size n_0 , however we will find that the physical observables are insensitive to the precise value of n_0 . This is in contrast to the oligomer size N which plays an important role in the phase behavior.

D. The monomer-oligomer-fibril assembly equilibrium

Now, we combine the free energies above into a grand canonical ensemble to determine how the assembly equilibria depend on the concentration of peptide monomers in solution. If the oligomeric state resembles a micelle, a reasonable approximation is that the oligomer species is dominated by a single aggregation number, with free energy given by Eq. 1. However, for the fibril, we assume a continuum of aggregation states having number n peptide chains and a free energy given by Eq. 5. To compute the properties of the solution,

we compute the *binding polynomial* [22],

$$Q = c_1 + c_1^N e^{\chi NL} + \gamma^{p\ell} \sum_n c_1^n g^{nL}, \quad (6)$$

In Eq. 6, c_1 is the concentration of monomers, $c_1^N e^{\chi NL}$ is the concentration of oligomers, and the final term is the sum over the concentrations of the fibrils of all possible lengths. The total peptide concentration, c_0 can be computed by using the concentration of each species and summing the number of peptides in each species. Thus, c_0 is written as

$$c_0 = \frac{dQ}{d \ln c_1} = c_1 + N c_1^N e^{\chi NL} + \gamma^{p\ell} \sum_{n=n_0}^{\infty} n c_1^n g^{nL}, \quad (7)$$

where n_0 is the smallest accessible fibril size.

The solution phase behavior is given by the peptide concentrations in each of three states: monomer, c_1 ; oligomer, c_{oligo} ; and fibril, c_{fibril} , where

$$c_{\text{oligo}} = N c_1^N e^{\chi NL} \quad (8)$$

and

$$c_{\text{fibril}} = \gamma^{p\ell} \sum_{n=n_0}^{\infty} n c_1^n g^{nL} \quad (9)$$

are the component terms from Eq. 7. The three relative concentration quantities, c_1/c_0 , c_{oligo}/c_0 and c_{fibril}/c_0 must sum to one. To compute the phase diagram we numerically solve Eq. 7 for c_1 at fixed values of c_0 , g , γ , and χ . The concentrations of peptides in the fibril and oligomer states are then computed from Eqs. 8 and 9. Fig. 5 shows the computed phase diagrams. The boundaries in Fig. 5 represent the conditions of equal populations of the two corresponding states. In the Methods section we derive analytic expressions for the phase boundaries. These are shown by the black lines in Fig. 5. The model predictions are given in the following section.

III. RESULTS

The model defined in the previous section leads to a free energy landscape with features schematically shown in Fig. 4. In the following we compute the phase equilibria resulting from this landscape.

A. The model predicts an *amyloid triple point*, a 3-state equilibria

Fig. 5 shows the phase diagram computed from Eq. 7. The x -axis shows the monomer concentration. The y -axis shows $\ln g/\chi$, the ratio of the free energy for a steric zipper to the free energy for amorphous hydrophobic aggregation. The model predicts three main features. First, increasing the amyloid peptide concentration in solution leads to increased aggregation (both oligomers and fibrils). Second, not surprisingly, at high peptide concentrations, changing solution conditions to favor steric zipping tips the balance from oligomers toward fibrils. This phase equilibrium line is relatively flat, indicating that it is not very dependent on monomer concentration. Third, there should be a triple point, a particular monomer concentration and solution condition at which monomers, oligomers, and fibrils are all present in equal populations.

The phase diagram can be closely approximated by comparing the critical fibril concentration (CFC) to the critical oligomer concentration (COC) (see Methods). The lesser of these two quantities determines the aggregate species that appears upon raising the peptide concentration. However, if the COC is less than the CFC it may be possible to drive the solution from the oligomer state to the fibril state by further raising the peptide concentration. This transition may be computed using the fibril-oligomer coexistence condition (see Eqs. 24 and 38). The converse is not true; it is not possible to reach the oligomer phase from the fibril phase by increasing the peptide concentration. This asymmetry arises from the definitions of the critical concentrations. The CFC is defined by the radius of convergence of Eq. 7, and thus it sets a hard limit on the achievable monomer concentration. On the other hand, the monomer concentration will still rise, albeit weakly, upon reaching the COC, and therefore it is possible for the monomer concentration to reach the CFC even after oligomers have begun to form provided the CFC is not much greater than the COC.

B. When fibrils are stable, oligomers are not.

Interestingly, the model predicts a ‘sponge-like behavior’: under fibril-forming conditions, amyloid peptide will be ‘soaked up’ into the fibrils and depleted from the oligomers. To see this, substitute the CFC, Eq. 16, into Eq. 8, to get

$$c_{\text{oligo}} \sim N e^{-LN(\ln g - \chi)}. \quad (10)$$

This small quantity, $e^{-(\ln g - \chi)} < 1$, is raised to a large power, LN . So, unless χ and $\ln g$ are closely matched, the concentration of the oligomeric state will be negligible under fibril-forming conditions. The implication for disease is that if oligomers are toxic, promoting fibril formation may deplete the toxins.

C. Fibril concentration increases as a nonlinear function of monomer concentration.

Fig. 6 compares the theory for how the fibril population, c_{fibril} , depends on peptide concentration, to the experiments of Terzi et al. [23]. Since the N-terminal 11-16 residues of A β are disordered [10, 24] in the fibril state, we take $L = 26$. In order to fit the data we convert the experimental concentration c_M (in Molar units) to the dimensionless concentrations required in our treatment. We use $c = (c_M/55.5)M$. From that fit, we find that $-L \ln g = -13.1$ and $-p\ell \ln \gamma = 15.5$ at the experimental conditions of 278 K and pH 7.4. This is an order of magnitude stronger than the per-residue binding energy within native proteins [8].

D. Fibril lengths undergo a ‘growth transition’ vs. monomer concentration.

Now we compute the distribution of fibril lengths. The probability $P(n)$ that a fibril has a length n is given by

$$P(n) = \frac{c_1^n g^{nL}}{\sum_i c_1^i g^{iL}}. \quad (11)$$

What are the average fibril lengths? In the Methods section we show that the average length scales as $c_0^{1/2} \gamma^{-\ell p/2}$, in agreement with the concentration dependence found in reference [26]. Fig. 7 shows the predictions of Eq. 26 compared to the average fibril-length measurements of van Raaij et al [25]. From the fit we find, g^L , which determines the onset of fibrillization and we find $\gamma^{\ell p}$, which determines the fibril length. We obtain $-L \ln g = -15.5$ and $-\ell p \ln \gamma = 32.3$. In α -synuclein fibrils, it is found that $p = 4$, twice the value of A β fibrils [25]. Accounting for this factor of two shows that the values of $L \ln g$ and $\ell \ln \gamma$ are quite similar to those determined for A β in the previous section. n_s and ℓ are not yet known for α -synuclein.

Fig. 8 shows the prediction that the fibril lengths follow an exponential distribution; see Eq. 26.

E. Denaturants destabilize the fibrils and oligomers

What is the effect of denaturants and osmolytes on amyloid aggregation? First, because both oligomers and fibrils are stabilized by hydrogen bonding and hydrophobic interactions, denaturants should ‘melt out’ amyloid aggregated states. A more subtle question is how denaturants shift the oligomer-fibril equilibrium. Fig. 9 shows the model predictions (1) that denaturants such as urea, not unexpectedly, should weaken hydrophobic and hydrogen bonding interactions, disrupting aggregation, (2) that more denaturant is required to disrupt aggregates if the amyloid concentration is high, and (3) that adding denaturant to fibrils can drive the system into the oligomer state.

We note two additional points. First, in apparent contradiction to this prediction, denaturants are sometimes used to promote fibrillization, but that appears to be observed exclusively in systems having a native folded state [27–29], unlike the systems we model here. Second, the present model resolves a paradoxical result in the literature. Chen and Glabe found that urea drove fibrils to ‘melt’ directly to monomers without passing through the oligomer state [4]. In contrast, Kim *et al.* found that urea drove fibrils to melt to oligomers, when then melted to monomers [30]. Our Fig. 9 gives an explanation: the A β peptide concentrations used by Kim *et al.* were 3-10-fold greater than those used by Chen and Glabe, shifting to a region of the phase diagram in which oligomers are a stable intermediate phase.

F. Electrostatic repulsion destabilizes the fibrils

To treat the effects of pH and salt, we express the binding free energy

$$-L \ln g(q, c_s) = -L \ln g_0 + \Delta F_{es}(q, c_s) \tag{12}$$

in terms of g_0 , which accounts for the binding energy for a reference peptide having zero net charge, and an electrostatic component, ΔF_{es} , which is the free energy of charging up the peptides from their uncharged state to a net charge q in the presence of a salt concentration c_s . The latter is given quantitatively by Eq 43.

Fig. 10 compares a simple calculation of the electrostatic repulsions with experimental measurements of dependence of the critical concentration, which we identify with the theoretical quantity $c_1^{(f)}$, on salt concentration. We compute a charge of $q = -3.9$ at pH 9.0 and $q = -2.8$ at pH 7.4 for the A β peptide [31]. We treat each peptide as a cylinder of radius $R = 10\text{nm}$ [32] using Poisson-Boltzmann theory; see Eq. 43. Fig. 10 shows two experiments: Klement et al. for pH 9 and Terzi et al. for pH 7.4. The sole fitting parameter in Fig. 10 is $-L \ln g_0 = -21.9$. This corresponds to $-L \ln g = -15.5$ under the pH 7.4, 5mM conditions of Terzi et al. This represents a good agreement with our previous result of $-L \ln g = -13.1$ given the extreme sensitivity of the electrostatic free energy at such low salt concentrations.

IV. CONCLUSION

We have described a general thermodynamic theory for the aggregation of short peptides into globular and fibrillar aggregates. The model predicts two transitions: (1) a micelle-like transition of monomeric peptides in solution to an oligomeric state involving a loose hydrophobic core and a loss of translational entropy, and (2) a transition from the disordered globular oligomeric state to an ordered β -structured fibrillar state, driven by tighter packing, hydrogen bonding, and steric and hydrophobic interactions.

We find good agreement of the model with experiments on fibril concentrations, average fibril lengths, and fibril length distributions *vs.* monomer concentrations. We find that the phase boundaries and transition states are highly sensitive to small changes in solution conditions and protein properties. Such sensitivities may be relevant to aggregation processes in amyloid diseases.

V. METHODS

Critical fibril concentration (CFC)

The concentration of peptides in the fibril state is given by the final term in Eq. 7

$$c_{fibril} = \gamma^{\ell p} \sum_{n=n_0}^{\infty} n c_1^n g^{nL} \quad (13)$$

$$= \gamma^{\ell p} c_1 g^L \frac{d}{d(c_1 g^L)} \sum_{n=n_0}^{\infty} c_1^n g^{nL} \quad (14)$$

$$= \gamma^{\ell p} \frac{n_0(1 - c_1 g^L)(c_1 g^{n_s \ell})^{n_0} + (c_1 g^L)^{n_0+1}}{(1 - c_1 g^L)^2}. \quad (15)$$

The sum in Eq. 13 converges when the argument is less than unity, therefore the monomer concentration must satisfy $c_1 < g^{-L}$ if the bulk concentration is to remain finite. This radius of convergence defines a concentration

$$c_1^{(f)} \sim g^{-L}, \quad (16)$$

which may be interpreted as the CFC for the fibril solution. For c_1 much less than this value the concentration of monomers in the fibril state c_{fibril} is strongly suppressed by the factor $\gamma^{\ell p} (c_1 g^L)^{n_0}$. However, as c_1 approaches g^{-L} the fibril concentration diverges. In this regime we can write $c_1 g^L = 1 - \delta$ and the fibril concentration becomes

$$c_{fibril} \simeq \gamma^{\ell p} \frac{(1 - n_0 \delta)(1 + n_0 \delta - \delta)}{\delta^2} \quad (17)$$

$$= \gamma^{\ell p} \frac{c_1 g^L + \mathcal{O}(\delta^2)}{(1 - c_1 g^L)^2}, \quad (18)$$

which demonstrates that c_{fibril} is insensitive to the lower limit n_0 .

Note that our definition for the CFC differs from that given in reference [26].

Critical oligomer concentration (COC)

Due to the importance of oligomers in disease progression, we would like to calculate the concentration of oligomers both in the presence and absence of fibrils. In the presence of fibrils we can approximate the concentration of peptides in the oligomer state, c_{oligo} , by using the CFC in the second term of Eq. 7 since the monomer concentration varies little in the vicinity of the fibril CFC

$$c_{oligo} \sim N g^{-LN} e^{\chi LN}. \quad (19)$$

This expression is only valid provided $e^{\chi} < g$. If this condition is not satisfied, then Eq. 2 is a monotonically increasing function of m meaning the oligomer state has a lower free energy per peptide than a fibril of any length. In this case no fibrils will be formed, and the

solution will be an equilibrium mixture of oligomers and monomers. We define the COC to be the concentration where the oligomer and monomer states have equal occupancies. Using the appropriate terms from Eq. 7 we find the COC given by

$$c_1^{(COC)} = \left(\frac{e^{-\chi NL}}{N} \right)^{1/(N-1)}. \quad (20)$$

Fibril-oligomer boundary

The boundary between the fibril and oligomer phases is defined, for points suitably removed from the monomer phase, by the condition $c_{fibril} = c_{oligo} \simeq c_0/2$. Using Eqs. 18 and 19 we have

$$c_0/2 = \gamma^{\ell p} \frac{c_1 g^L}{(1 - c_1 g^L)^2} \quad (21)$$

$$c_0/2 = N c_1^N e^{\chi NL}. \quad (22)$$

Eq. 21 yields a recursive formula for c_1 , which to lowest order gives

$$c_1 \simeq g^{-L} (1 - \sqrt{2\gamma^{\ell p}/c_0}) \quad (23)$$

which can be combined with Eq. 22 to yield a condition for the phase boundary

$$\frac{\ln g}{\chi} = \frac{NL \ln g}{\ln \left(\frac{c_0}{2N g^{-L}} \right) - N \ln \left(1 - \sqrt{2\gamma^{\ell p}/c_0} \right)}. \quad (24)$$

This expression is plotted with long dashes in Fig. 5

Average fibril length

The critical concentrations for fibril and oligomer formation, $c_1^{(f)}$ and $c_1^{(o)}$ are notably lacking a dependence on the nucleation parameter γ . While this parameter has little effect on the relative stability of the fibril and oligomer phases, we expect that it will play a large role in determining the equilibrium lengths of mature fibrils. To see this we consider a system that is deep within the regime where fibrils are the dominant species so that $c_0 \simeq c_{fibril}$. Using Eq. 18 we find

$$c_1 \simeq g^{-L} (1 - \sqrt{\gamma^{\ell p}/c_0}). \quad (25)$$

The j th moment of the fibril length distribution is given by

$$\langle n^j \rangle = \frac{\gamma^{\ell p} \sum_n n^j c_1^n g^{nL}}{\gamma^{\ell p} \sum_n c_1^n g^{nL}} \quad (26)$$

$$= \left(\frac{(c_1 g^L)^{n_0}}{1 - c_1 g^L} \right)^{-1} \left(c_1 g^L \frac{d}{d(c_1 g^L)} \right)^j \left(\frac{(c_1 g^L)^{n_0}}{1 - c_1 g^L} \right). \quad (27)$$

The average length is given by the first moment $j = 1$

$$\langle \ell \rangle = n_0 + \frac{c_1 g^L}{1 - c_1 g^L} \quad (28)$$

$$\sim c_0^{1/2} \gamma^{-\ell p/2} + \text{const}, \quad (29)$$

where Eq. 25 has been used to extract the scaling behavior.

The lack of a dependence on g in this scaling relation is a result of an approximation based on $c_0 \gg c_1^{(f)}$. When this assumption is satisfied the large majority of protein is in the fibril state, and the problem of determining the fibril lengths is reduced to a question of fibril breakage statistics. Since each breakage incurs a statistical penalty $\gamma^{\ell p}$, the functional form of Eq. 29 is not surprising (the factor of two in the exponent is a result of the degeneracy of breakage points). For systems near the onset of fibrillization $c_0 \simeq c_1^{(f)}$ the fibril lengths depend sensitively on g and Eq. 26 must be used to model the lengths.

Denaturants

Denaturants destabilize the folded states of proteins by weakening hydrophobic interactions and peptide-peptide H-bonds relative to peptide-solvent H-bonds [33]. To capture the effect of denaturants on the interaction free energy quantities g and γ , we use

$$\begin{aligned} kT \ln g_c &= kT(\ln g - a_0 c_d) \\ kT \ln \gamma_c &= kT(\ln \gamma + a_0 c_d), \end{aligned} \quad (30)$$

where g_c and γ_c are the propagation parameters in the presence of denaturant, c_d is the denaturant concentration and a_0 is a constant describing the destabilizing effect of the osmolyte. This form reflects the fact that the denaturant weakens the H-bonds captured in g , but also reduces the fibril end free energy $-\ln \gamma$, which arises largely from unsatisfied H-bonds.

Using Eqs. 16, 20, and 30 we can compute how the critical concentrations will shift as a function of denaturant concentration. At the onset of fibrillization we have $c_0 = c_1^{(f)}$, so from Eqs. 16 and 30 we have

$$\ln c_1 = -L \ln g_c \quad (31)$$

$$= -L(\ln g - a_0 c_d), \quad (32)$$

which can be solved for c_d to give the phase boundary

$$c_d = \frac{\ln c_0 + L \ln g}{L a_0}. \quad (33)$$

Similarly, for the oligomer state we write

$$\chi_c = \chi - a_1 c_d \quad (34)$$

where a_1 has been introduced to reflect the fact that since the oligomers are more dependent on hydrophobic interactions and less dependent on H-bonds for stability, and therefore, the destabilization coefficient will, in general, be different. The onset of oligomerization may be determined from Eq. 20

$$c_0 = \left(\frac{e^{-NL(\chi - a_1 c_d)}}{N} \right)^{1/(N-1)}, \quad (35)$$

which can be rearranged to yield

$$c_d = \frac{1}{a_1} \left(\chi + \frac{(N-1) \ln c_0 + \ln N}{NL} \right). \quad (36)$$

The fibril-oligomer boundary can be derived from Eqs. 21 and 22

$$\ln c_0/2N = NL(\chi - a_1 c_d) - NL(\ln g - a_0 c_d), \quad (37)$$

where we have dropped the correction term in Eq. 21. In Fig. 9 we take $a_1 = a_0/2$ reflecting our expectation that the hydrophobic interactions stabilizing the oligomer are less affected by the presence of denaturant than the H-bonds stabilizing the fibril [8, 34]. However, the particular choice of $a_0/2$ is for illustration purposes. With this approximation for a_1 Eq. 37 becomes

$$c_d = \frac{2}{a_0 NL} \left(\ln \frac{c_0}{2N} - NL(\chi + \ln g) \right). \quad (38)$$

Based on denaturation studies, we expect that $a_0 = 0.022M^{-1}$ for urea and 0.042 for guanidinium [8]. Using our estimates of $L \ln g = 13.1$ and $\ell p \ln \gamma = -15.5$ (in the absence of urea) for $A\beta$ from our previous analysis of fraction fibril as a function of concentration (Fig. 6) we can predict the fibril fraction as a function of urea using Eq. 30 without a fit parameter. Our prediction is compared with the experimental data in Table I.

Electrostatics

To compute F_{es} we approximate the fibril as a smooth cylinder of radius R and uniform charge density. The linear charge density may be computed by noting that the average charge per β -strand is q/n_s and there are $2p$ strands per layer in the fibril.

To determine the peptide charge as a function of pH, we use

$$q = \sum_i^{\text{acidic residues}} -\frac{10^{pH-pK_{a_i}}}{1 + 10^{pH-pK_{a_i}}} + \sum_i^{\text{basic residues}} +\frac{10^{pK_{a_i}-pH}}{1 + 10^{pK_{a_i}-pH}}, \quad (39)$$

	Experiment [30]		Theory
[urea]	Oligomer fraction	Fibril fraction	Fibril fraction
0.4M	0	0.37	0.30
2	0.37*		0.03
4	0.2	0	10^{-3}
6	0.22	0	10^{-5}

TABLE I: Computed fraction of peptide in the fibril phase compared to the data of Kim *et al.* [30].

* Aggregate fraction was observed to be a combination of fibrils and oligomers.

where the pKas of the amino acids are taken from Ref. [31]. So, the charge density on each peptide-molecule cylinder is $\rho = 2qp/n_s a$, where $a = 4.7 \text{ \AA}$ is the spacing between amino acids.

We then solve for the electrostatic potential ψ using the Poisson-Boltzmann equation

$$\epsilon \frac{1}{r} \frac{\partial}{\partial r} r \frac{\partial \psi}{\partial r} = -e(c_+ - c_-), \quad (40)$$

where the ion concentrations are $c_{\pm} = c_s e^{\mp e\psi/kT}$. In the linearized (Debye-Huckel) approximation, Eq. 40 has the solution

$$\psi(r) = \frac{2q}{2\pi R a \epsilon \kappa K_1(\kappa R)} K_0(\kappa r), \quad (41)$$

however, we use the numerical solution of the nonlinear Eq. 40 as the dimensionless potential $e\psi/kT$ can reach values in excess of unity at the low salt concentrations we consider. Here κ^{-1} is the Debye length, defined via $\kappa^2 \equiv 2e^2 c_0 / (\epsilon k_B T)$. At infinite dilution the appropriate boundary conditions are $\psi'(R) = -\rho/2\pi\epsilon R$ and $\psi(\infty) = 0$, but for the purposes of the numerical solver we employ the outer boundary condition $\psi'(d) = 0$ corresponding to a solution of fibrils separated by an average distance $2d$. We take $d = R + 5\kappa^{-1}$ (see Fig. 11). For $d \gg \kappa^{-1}$ the influence of the outer boundary condition will be minimal.

Once we have computed ψ , we get the electrostatic free energy density of the peptide cylinder as [35]

$$f = \frac{\epsilon}{2} \left(\frac{d\psi}{dr} \right)^2 + kT(c_+ \ln(c_+/c_s) + c_- \ln(c_-/c_s) - c_+ - c_- + 2c_s). \quad (42)$$

The first term in Eq. 42 is the electrostatic energy stored in the electric field, and the remaining terms account for the translational entropy of the ions in the screening layer. We then compute the free energy per peptide using

$$\Delta F_{es} = 2\pi \frac{n_s a}{2p} \int_R^\infty f(r) r dr \quad (43)$$

where r is the radial coordinate perpendicular to the axis of the cylinder.

-
- [1] C. M. Dobson, *Nature* **426**, 884 (2003).
 - [2] J. Hardy and D. J. Selkoe, *Science* **297**, 353 (2002).
 - [3] S. Chimon *et al.*, *Nat. Struc. Mol. Bio.* **14**, 1157 (2007).
 - [4] Y. Chen and C. Glabe, *J. Biol. Chem.* **281**, 24414 (2006).
 - [5] C. Glabe, *J. Biol. Chem.* **283**, 29639 (2008).
 - [6] K. Dill, *Biochemistry* **24**, 1501 (1985).
 - [7] K. Dill and D. Stigter, *Adv. Prot. Chem.* **46**, 59 (1995).
 - [8] K. Ghosh and K. Dill, *Proc. Nat. Acad. Sci.* **106**, 10649 (2009).
 - [9] R. Nelson *et al.*, *Nature* **435**, 773 (2005).
 - [10] T. Luhrs *et al.*, *Proc. Nat. Acad. Sci.* **102**, 17342 (2005).
 - [11] M. Sawaya *et al.*, *Nature* **447**, 453 (2007).
 - [12] C. Wasmer *et al.*, *Science* **319**, 1523 (2008).
 - [13] B. Zimm and J. Bragg, *J. Chem. Phys.* **31**, 526 (1959).
 - [14] J. Schellmann, *J. Phys. Chem.* **62**, 1485 (1958).
 - [15] S. Lifson and A. Roig, *J. Chem. Phys.* **34**, 1963 (1961).
 - [16] D. Poland and H. Scheraga, *Theory of Helix-Coil Transitions in Biopolymers* (Academic Press, New York, 1970).
 - [17] K. Ghosh and K. Dill, *J. Am. Chem. Soc.* **131**, 2306 (2009).
 - [18] S. Auer, F. Meersman, C. Dobson, and M. Vendruscolo, *PLOS Comp. Biol.* **4**, e1000222 (2008).
 - [19] J. Jarrett, E. Berger, and P. Lansbury, *Biochemistry* **32**, 4693 (1993).
 - [20] J. Zhang and M. Muthukumar, *J. Chem. Phys.* **130** (2009).
 - [21] T. Serio *et al.*, *Science* **289**, 1317 (2000).

- [22] K. Dill and S. Bromberg, *Molecular Driving Forces* (Garland Science, New York, NY, 2002).
- [23] E. Terzi, G. Holzemann, and J. Seelig, *J. Mol. Bio.* **252**, 633 (1995).
- [24] A. Petkova *et al.*, *Proc. Nat. Acad. Sci.* **99**, 16742 (2002).
- [25] M. van Raaij, J. van Gestel, I. Segers-Nolten, S. W. de Leeuw, and V. Subramaniam, *Biophys. J.* **95**, 4871 (2008).
- [26] C. Lee, *Phys. Rev. E* **80**, 031922 (2009).
- [27] D. Hamada and C. Dobson, *Prot. Sci.* **11**, 2417 (2002).
- [28] A. Ahmad, I. Millett, S. Doniach, U. VN, and A. Fink, *J. Biol. Chem.* **279**, 14999 (2004).
- [29] S. Wang, Y. Hung, P. Wang, and J. Wu, *Korean J. Chem. Eng.* **24**, 787 (200).
- [30] J. Kim, A. Muresan, K. Lee, and R. Murphy, *Prot. Sci.* **13**, 2888 (2004).
- [31] A. Sillero and J. Ribeiro, *Analytical Biochemistry* **179**, 319 (1989).
- [32] K. Klement *et al.*, *J. Mol. Biol.* **373**, 1321 (2007).
- [33] M. Auton, L. M. F. Holthauzen, and D. W. Bolen, *Proc. Nat. Acad. Sci.* **104**, 15317 (2007).
- [34] D. Bolen and G. Rose, *Ann. Rev. of Biochem* **77**, 339 (2008).
- [35] D. Andelman, *Proceedings of the Nato ASI & SUSSP on "soft condensed matter physics in molecular and cell biology"* (Taylor & Francis, New York, 2006), chap. Introduction to electrostatics in soft and biological matter, pp. 97–122.

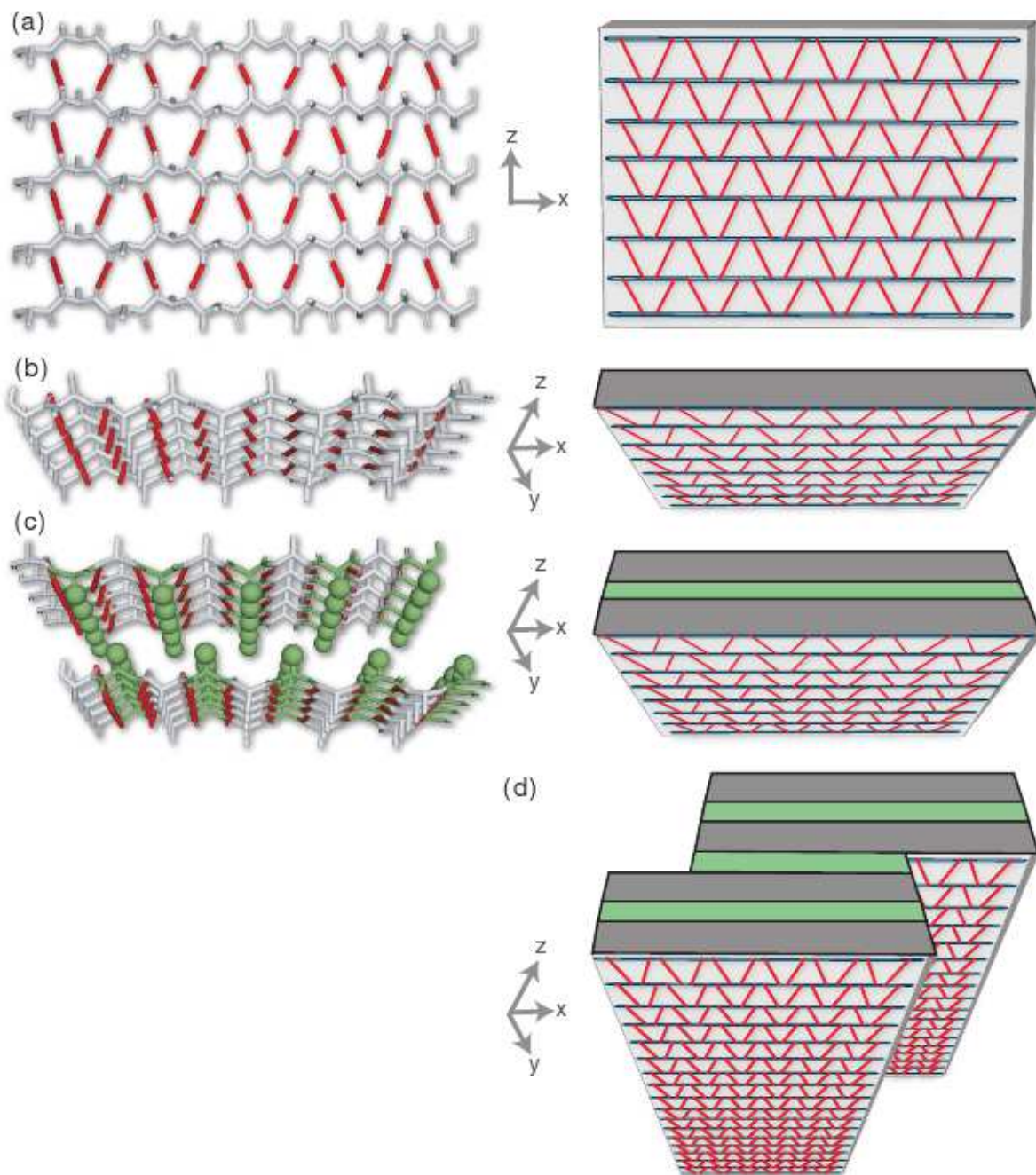


FIG. 1: Assembly hierarchy of amyloid fibrils shown in atomistic cartoon representation (left) and schematically with β -sheets as blocks (right). a) A single β sheet comprised of parallel β -strands. b) β -sheet observed along fibrillization axis. c) Assembled β -sandwich (protofilament) consisting of two β -sheets. Note the steric zipper interactions shown as interdigitating side chains (left) and as a green layer (right). d) Mature fibril consisting of $p = 2$ protofilaments.

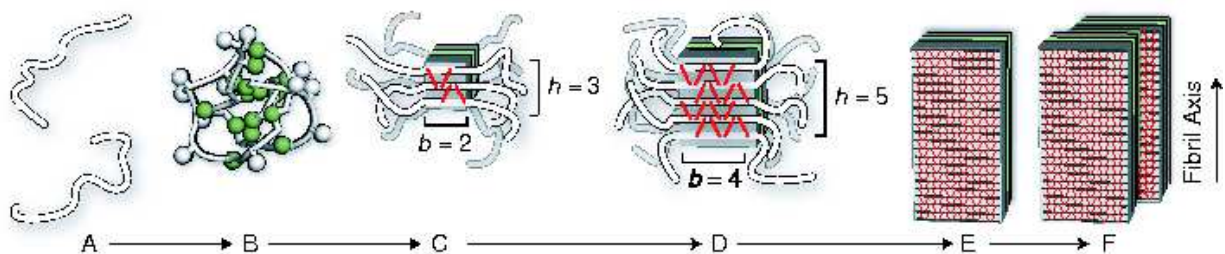


FIG. 2: Model of amyloid aggregation equilibria. Each black line indicates the peptide backbone. Each red line shows one hydrogen bond. A) Isolated peptide monomers in solution. B) Oligomeric assembly of a few peptide chains. C) Nucleus of β -sheet structure. The peptide backbone runs perpendicular to the fiber axis. D) Post-critical nucleus structure having more β -structure. E) *Protofilament* is a single long thread of β -structure consisting of a β -sandwich, two β -sheet planes face-to-face. F) *Full fibril*, a bundle of protofilaments, shown here containing $p = 2$ protofilament threads.

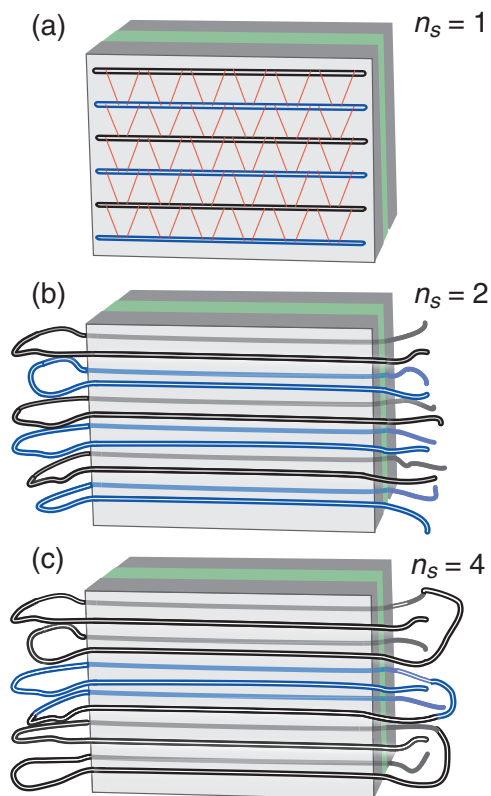


FIG. 3: Schematic representation of the parameter n_s . Here each peptide chain contributes a) one, b) two, and c) four β -strands to the fibril. For clarity, adjacent peptide chains are shown in alternating colors.

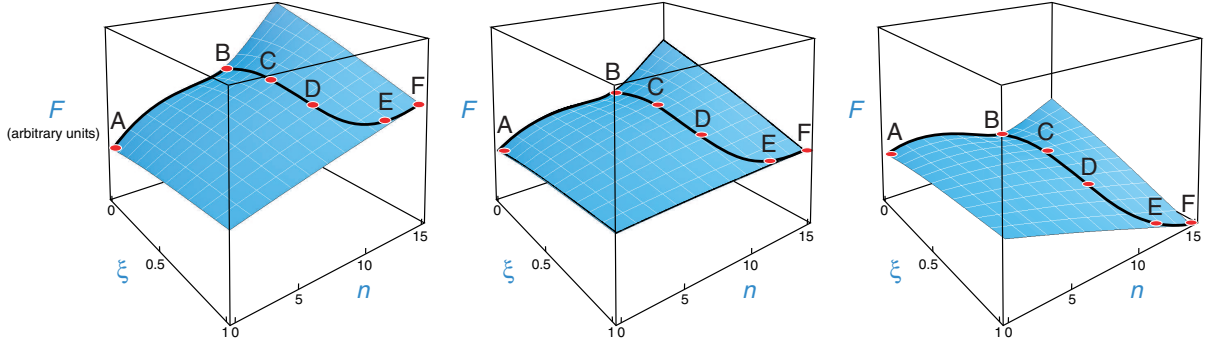


FIG. 4: Schematic representation of the free energy landscape described by our model at low (left), intermediate (middle), and high peptide concentration (right). Labels correspond to the states shown in Fig. 2. At low concentrations the monomer state (A) is the free energy minimum, while at high concentrations the fibril (F) is the minimum. At intermediate concentrations the solution is an equilibrium of monomers and oligomers (B).

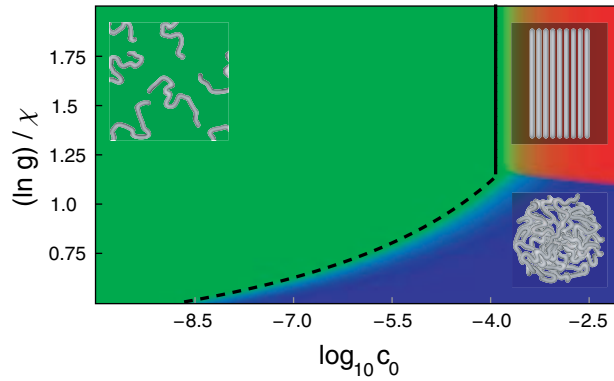


FIG. 5: Phase diagram for peptides with $p, n_s = 1$, $\ell = 15$, $\ln g = 0.6$, and $\ln \gamma = -2$ as a function of peptide concentration and $\ln g / \chi$. Green = c_1 / c_0 (monomers). Blue = c_{oligo} / c_0 (oligomers). Red = c_{fibril} / c_0 (fibrils). Lines depict phase boundaries computed from Eq. 24 (long dashes), Eq. 20 (short dashes), and Eq. 16 (solid).

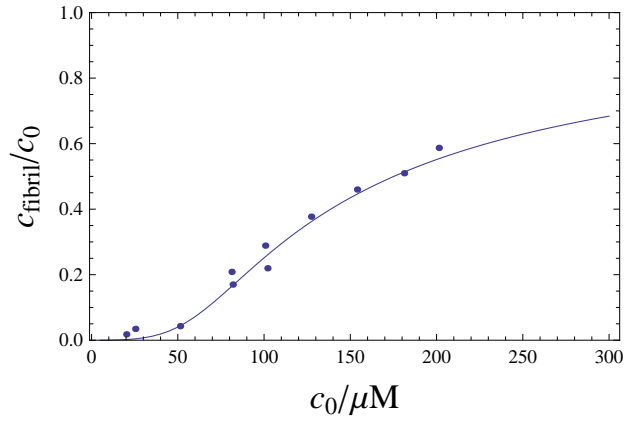


FIG. 6: Plot of c_{fibril} as a function of the bulk peptide concentration compared to CD data of Terzi *et al.* for $\text{A}\beta_{1-40}$ [23]. $L = 26$, $n_s = 2$, $p = 2$, $g = 1.66$ and $\gamma = 0.54$

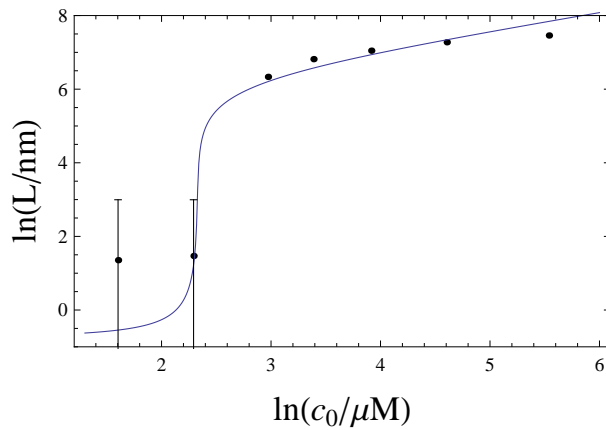


FIG. 7: Average length of fibrils *vs.* peptide concentration, and compared to experiments on α -synuclein [25].

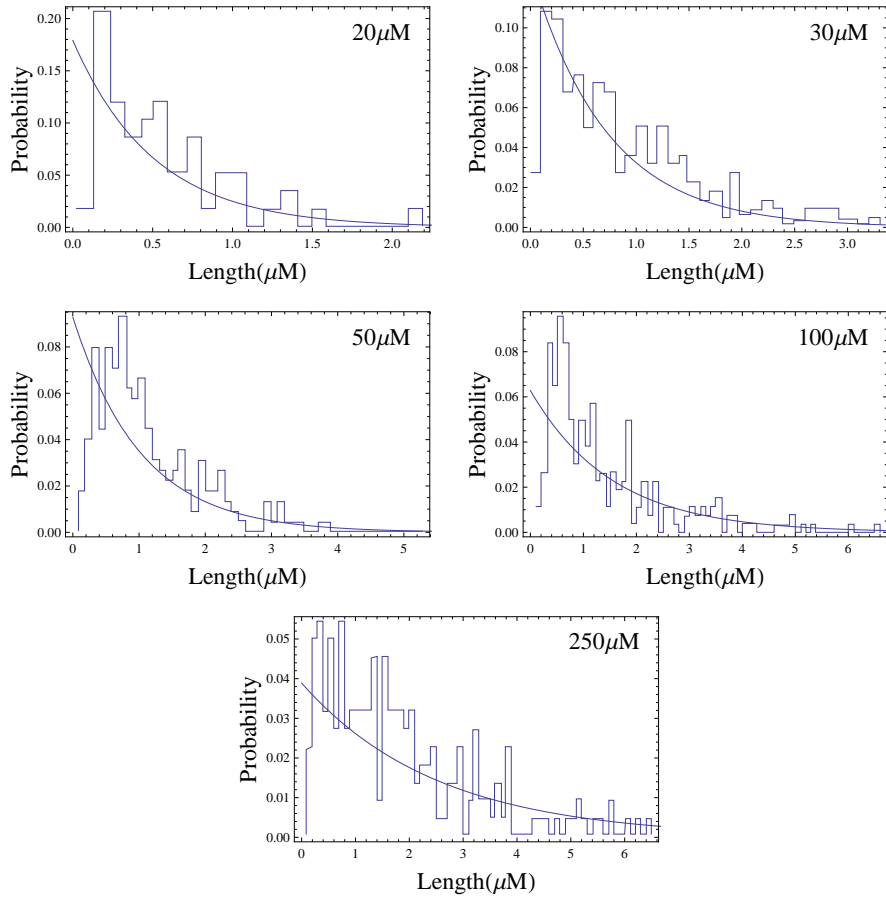


FIG. 8: Comparison of the computed fibril length distribution as a function of the bulk peptide concentration to the experimental distributions of α -synuclein [25].

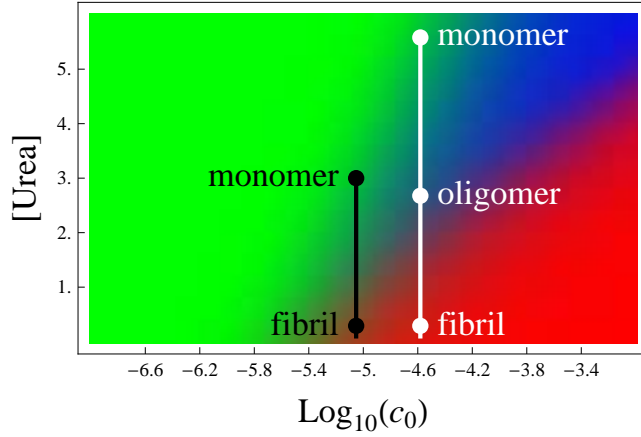


FIG. 9: Phase diagram for $A\beta$ as a function of peptide concentration and urea concentration. The colors represent monomers (green), oligomers (blue), and fibrils (red). $N = 4$, $\chi NL = 36.4$ [4], and all other parameters are identical to Fig. 6. This diagram explains a discrepancy between the experiments of Chen and Glabe, where the black line indicates denaturation. They found no intermediate oligomers. For the Kim experiments, denaturation is indicated by the white line; they observed oligomeric intermediates.

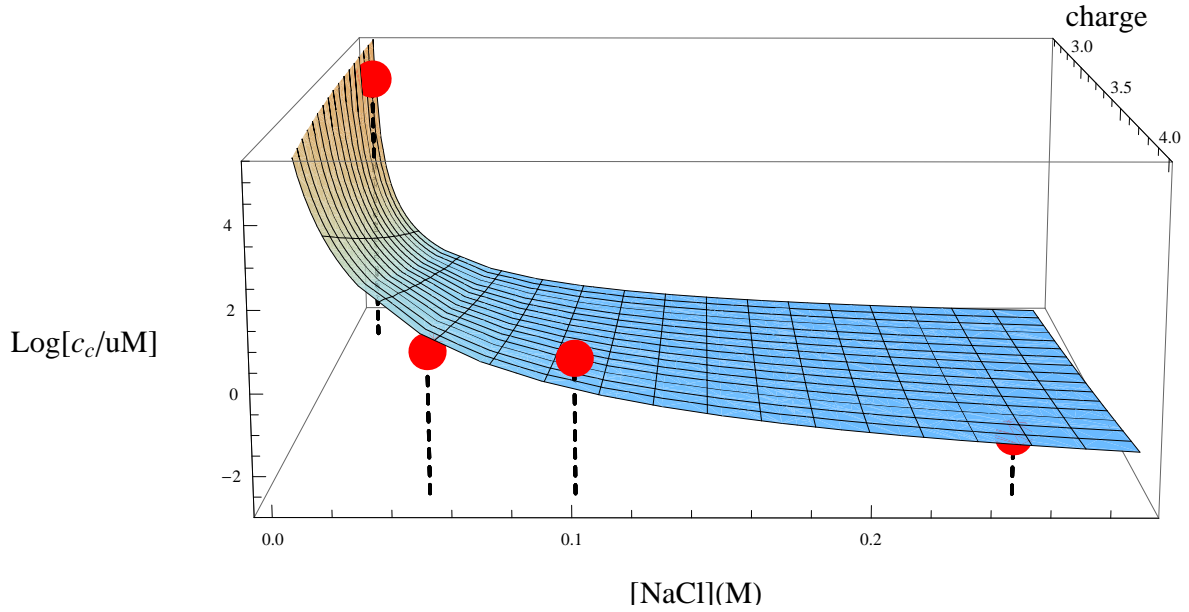


FIG. 10: Predicted solubility of $A\beta_{40}$ as a function of salt concentration and net peptide charge. Data points at $q = 3.9$ are from [32] and the point at $q = 2.8$ is from [23].

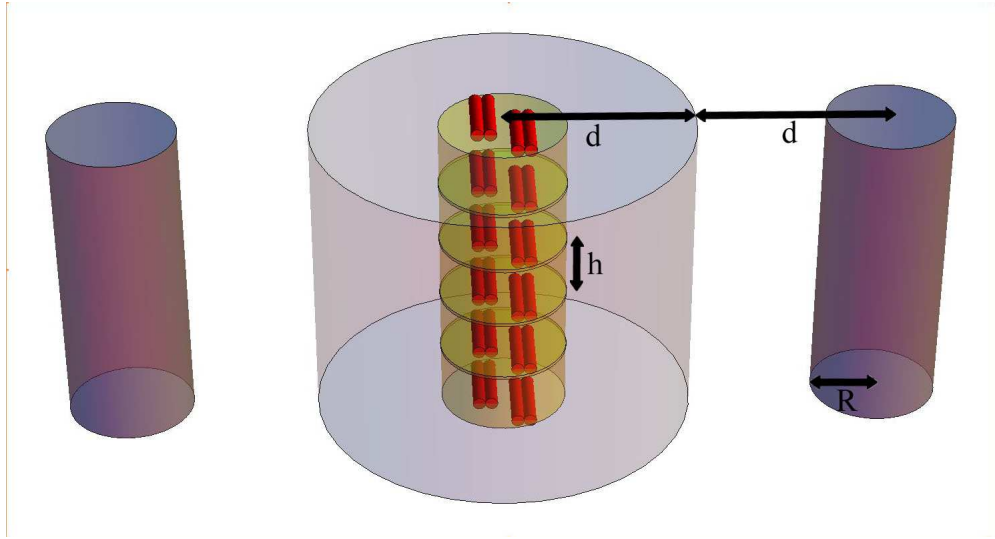


FIG. 11: Cylindrical fibril geometry used to solve Eq. 40. Fibrils are taken as cylinders of radius R separated by a distance $2d$. Red lines denote individual β -strands (shown here for a fibril with $p = 2$). Horizontal disks show the spacing h between β -strand layers within the fibril. Eq. 40 is solved from surface of the reference fibril (center), out to a distance d (outer cylinder) with the boundary condition $\psi'(d) = 0$ reflecting the symmetry of the electric potential between the cylinders.